This is the **peer reviewed version** of the following article: *Journal of Computational Chemistry* 2018, 39, 1413- 1423, which has been published in final form at: https://doi.org/10.1002/jcc.25209

Dispersion interactions between neighboring Bi atoms in $(BiH_3)_2$ and $Te(BiR_2)_2$

Rebekka Haack*, Stephan Schulz†, Georg Jansen‡

January 21, 2018

Abstract

Triggered by the observation of a short Bi···Bi distance and a Bi-Te-Bi bond angle of only 86.6° in the crystal structure of Bis(diethylbismuthanyl)Tellurane quantum chemical computations on interactions between neighboring Bi atoms in $Te(BiR_2)_2$ molecules (R=H, Me, Et) and in $(BiH_3)_2$ were undertaken. Bi···Bi distances atoms were found to significantly shorten upon inclusion of the d shells of the heavy metal atoms into the electron correlation treatment, and it was confirmed that interaction energies from spin component-scaled second-order Møller-Plesset theory (SCS-MP2) agree well with coupled-cluster singles and doubles theory including perturbative triples (CCSD(T)). Density functional theory-based symmetry-adapted perturbation theory (DFT-SAPT) was used to study the anisotropy of the interplay of dispersion attraction and steric repulsion between the Bi atoms. Finally, geometries and relative stabilities of syn-syn and syn-anti conformers of $Te(BiR_2)_2$ (R=H, Me, Et) and interconversion barriers between them were computed.

Keywords: Bismuthine dimer, Bis(dialkylbismuthanyl)Tellurane, Dispersion interactions, Steric repulsion, SAPT

*Faculty of Chemistry, University Duisburg-Essen, Universitätsstr. 5, 45117 Essen, Germany
†Faculty of Chemistry, University Duisburg-Essen, Universitätsstr. 5, 45117 Essen, Germany
‡Faculty of Chemistry, University Duisburg-Essen, Universitätsstr. 5, 45117 Essen, Germany

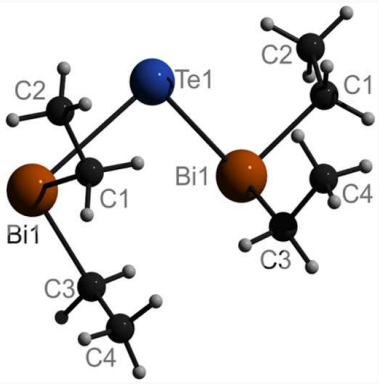

Triggered by experimental observations of a short Bi$\cdots$Bi distance and a very small Bi-Te-Bi bond angle in $Te(BiEt_2)_2$ the interplay of dispersion attraction and steric repulsion between neighboring bismuth atoms is investigated through quantum chemical calculations of the $(BiH_3)_2$ model system and of $Te(BiR_2)_2$ molecules (R=H, Me, Et). Syn-syn and syn-anti conformers of $Te(BiR_2)_2$ are found to be energetically close and to interconvert easily.

INTRODUCTION

Recent years witnessed a change in the perception of bulky functional groups from causing steric hindrance to also creating attractive forces between molecules or parts of a molecule[1]. The physical reason for this attraction is known as the dispersion force and is, in the language of quantum chemistry, due to dynamical electron correlation. In recent years, dispersion interactions were identified as one major structure directing force in inorganic and in metal organic complexes and a reasonable number of compounds have been found, in which dispersion forces play a key role in their chemical behavior[2–4]. In most of these complexes - often containing heavy main group metal atoms - attractive intermolecular interactions between the sterically demanding organic substituents have been studied, in particular H$\cdots$H interactions between C-H moieties in the organic ligands. In contrast, attractive intermolecular and intramolecular metal$\cdots$metal interactions have been investigated to a far lesser extent. While organic ligands without hetero atoms may become good dispersion energy donor (DEDs) upon an accumulation of atoms, *t*-butyl and adamantyl groups forming prominent examples, heavy metal atoms with fully filled d shells accumulate a high number of electrons in a relatively small volume. The well-known "aurophilic"[5–10] or more general "metallophilic" interactions demonstrate the potential of heavy metal atoms to maximize dispersion interactions while keeping the DED volume low. Molecules containing heavier main group metal atoms of group 15 (Sb, Bi) and group 16 (Te) are ideal candidates for the design of systems of "high-density dispersion energy donors". For instance, low-valent distibines (R_2Sb-SbR_2) and dibismuthines (R_2Bi-BiR_2) as well as ditellanes (Te$_2$R'$_2$), in which the metal atoms adopt the formal oxidation state +II and +I, respectively, and in which mainly valence-shell p orbitals are involved in the formation of covalent bonds, are known to form relatively strong intermolecular metal$\cdots$metal interactions in the solid state[6], typically resulting in interatomic metal$\cdots$metal distances in the range 350 - 400 pm (Fig. 1).

These intermolecular interactions, which are mainly based on dispersion interactions, can significantly influence the physical and chemical properties of the resulting compounds as can clearly be seen in tetraalkyldistibines and -dibismuthines with sterically less demanding organic substituents. The bond angles between the ligands in complexes of these heavy metal

atoms often approach 90 degrees around the central pnictogen and chalcogen atoms, mainly resulting from the low-lying s-orbital and hence the high p-character of the bonding electron pairs. As a consequence, they are fairly exposed and therefore favor close intermolecular contacts, often yielding chain-like structures in the solid state with short intermolecular metal$\cdots$metal contacts below the sum of the van-der-Waals radii[11], which are typically interrupted upon melting, resulting in a bathochromic shift - the so-called "thermochromic" effect - between fluid and solid phases[12]. Unfortunately, whether a given compound will be thermochromic or non-thermochromic is still not predictable. For instance, Sb_2Me_4 and Bi_2Me_4 are both thermochromic, whereas the Et-substituted compounds are either thermochromic (Sb_2Et_4) or non thermochromic (Bi_2Et_4), respectively. Moreover, it is still questionable if the thermochromic effect is exclusively based on the breakage of intermolecular metal$\cdots$metal bonds. For instance, Et_4Sb_2 reversibly forms a yellow and a red phase in the solid state and surprisingly, the solid state structures of both phases and the intermolecular distances are almost identical[13,14] Therefore, the different colors of both phases in this specific case must originate from other effects, which are still unknown. In addition to as-mentioned homometallic group 15 compounds of the type M_2R_4, heterometallic group 15/16 compounds such as Te-bridged compounds of the type R_2M-Te-MR_2 (M = Sb, Bi)[15–17] as well as compounds of the general type R_2MTeR' (M = Sb, Bi; R = Me, Et, R' = Me, Ph)[18–23], also show intermolecular contacts in the solid state, resulting in thermochromic behavior[24]. Early quantum chemical studies on distibines and dibismuthines demonstrated that there is no intermolecular binding on the Hartree-Fock level of theory[25], while with second-order Møller-Plesset perturbation theory (MP2) the interaction potentials became attractive, with computed dimerization energies in the range 8 - 13 kJ/mol[26]. Even though the intermolecular Sb$\cdots$Sb force constant in the dimer on the MP2 level was underestimated by a factor of more than two as compared to the measured solid-state result[27], the computations suggest that intermolecular interactions between small molecules containing heavier pnictogen atoms may become about as strong as, e.g., the CH$\cdots$N hydrogen bridge in the acetylene-ammonia dimer[28]. As concerning the reasons for the strength of these interactions, it was concluded that in analogy to metallophilic interactions between closed-shell metal ions they were largely caused by dispersion interactions, which at least qualitatively are taken

into account at the MP2 level of theory.

However, distibines and dibismuthines are not only of particular interest due to their tendency to form intermolecular metal$\cdots$metal interactions in the solid state but also due to their capability to serve as starting reagents for the formation of metal-centered radicals. For instance, persistent stibinyl and bismuthinyl radicals R_2Sb and R_2Bi (R_2 = 1,1,4,4-tetrakis-(trimethylsilyl)butane-1,4-diyl) were generated from the corresponding distibine and dibismuthine R_2M-MR_2, which have extraordinarily long M-M bonds and dissociate reversibly into the corresponding pnictogen-centered radicals in solution[29]. The release of accumulated strain energy within the dimers has been made responsible as the driving force for the dissociation to monomers ("Jack-in-the-Box" molecular model). However, Power *et al.* recently investigated[30] the dissociation of diphosphanes and diarsanes $[:M\{CH(SiMe_3)_2\}_2]_2$ (M = P, As) and $[:M\{N(SiMe_3)_2\}_2]_2$ containing sterically demanding bis(trimethylsilyl)methanide and bis(trimethylsilyl)amide substituents into the corresponding monomeric radicals ($\cdot M\{CH(SiMe_3)_2\}_2$, $\cdot M\{N(SiMe_3)_2\}_2$) by quantum chemical methods. The dispersion-corrected density functional theory (DFT+D) method B3PW91D3 was included to particularly estimate dispersion force effects. Negative dissociation energies of 43.1 (P) and 27.2 kJ/mol (As) were calculated for the diphosphane and diarsane without the dispersion correction, indicating that the radical monomers are more stable, whereas the incorporation of dispersion force effects afforded high, positive dissociation energies of +157.3 (P) and +155.2 kJ/mol (As) that favored dimeric structures. These calculations clearly showed that attractive dispersion forces could exceed those of ligand relaxation and stabilize the dimeric structures. As a consequence, the balance of dispersion forces and entropic effects are the major determinants of the dissociation equilibria of such compounds[30].

While DFT+D methods[31] in general allow to obtain reasonable total intermolecular interaction energies, the dispersion correction contained in these depends on the choice of the exchange-correlation functional and the damping function used to join the long-range and short-range parts of the electron correlation contribution, the former stemming from the dispersion correction, the latter more or less already contained in the functional. It thus in general provides only a qualitative measure of the importance of dispersion. This can be remedied through dispersionless DFT (dlDFT)[32], in which 100% of the dispersion en-

ergy have to come from elsewhere, e.g., from symmetry-adapted intermolecular perturbation theory (SAPT)[33–36] or from model expressions fitted to the SAPT dispersion contribution. This is also the case for the Pauli-Blockade (PB) method[37] which self-consistently describes mutual polarization of one monomer through the other on the DFT level. Systematic applications of one of these methods to compounds containing heavy group 15 and 16 metals so far seem not to be available. SAPT also has only rarely been applied to compounds containing heavy metals, with the notable exception of aurophilic interactions[38,39], where unreasonably large induction contributions indicate overpolarization and thus divergence of the perturbation series. But even in this extreme case the dispersion and exchange-dispersion contributions appear to be sound. SAPT based on a description of the monomers through DFT (DFT-SAPT)[36] recently has been used to show that the attractive part of the interactions between $SbCl_3$ and the π systems of benzene, toluene and hexamethylbenzene is dominated by dispersion, yet very strongly enhanced by electrostatic and induction contributions[40]. Second-order Møller-Plesset theory (MP2), which has been used to study Bi$\cdots\pi$ interactions[41], is the most efficient among the supermolecular wavefunction-based *ab initio* electron correlation approaches. However, it is known to overestimate the dispersion contribution and thus to overbind pnictogen- and chalcogen-containing molecular complexes[42] as compared to the "gold standard" of single and double excitation coupled-cluster theory including perturbative triple excitations (CCSD(T)). The spin-component-scaled variant of MP2 (SCS-MP2)[43], on the other hand, leads to strongly improved interaction energies[42]. In all of the mentioned supermolecular and SAPT calculations effective core potentials (ECPs)[44] were used to account for relativistic effects and to reduce the number of electrons.

In an extension of our preliminary work on rather strong dispersion-dominated intermolecular Te$\cdots$Sb and Te$\cdots$Bi interactions in $Et_2SbTeEt$ and $Et_2BiTeEt$ (-51.6 and -65.6 kJ/mol)[45], we synthesized and investigated compounds of the general type $R_2Sb\text{-}E\text{-}SbR_2$ (E = S, Se, Te)[46]. The Te-bridged derivatives were of particular interest since they show thermochromic behavior, which most likely results from the presence of intermolecular Sb$\cdots$Sb (3.673 Å) and Sb$\cdots$Te contacts (3.625 Å) as observed in the solid state structure. Moreover, the analogous Bi compounds and $R_2Bi\text{-}E\text{-}BiR_2$, which were also structurally characterized by single crystal X-ray diffraction, did not exhibit any thermochromic behavior, which coin-

cides with the absence of any intermolecular Bi$\cdots$Bi contacts in the solid state[47]. The most noticeable difference in the solid state structures of $Te(SbMe_2)_2$, $Te(SbEt_2)_2$ and $Te(BiEt_2)_2$ are their different conformations. $Te(SbEt_2)_2$ adopts a syn-anti orientation in the solid state, whereas $Te(SbMe_2)_2$ and $Te(BiEt_2)_2$ crystallize as syn-syn conformers (Fig. 2). Comparable findings were observed in the solid state structures of bis(dimethylstibanyl)oxane $O(SbMe_2)_2$ (syn-anti conformer) and -sulfane $S(SbMe_2)_2$ (syn-syn conformer)[48]. Moreover, GED studies by Haaland *et al.* showed that bis(dimethylstibanyl)oxane and -sulfane $E(SbMe_2)_2$ exist as syn-syn and syn-anti conformers in the gas phase (syn-anti concentrations: E = O 51(7)%; E = S 48(4)%), whereas the presence of syn-anti conformers for the heavier homologues (E = Se, Te) was uncertain[49,50]. DFT calculations revealed that the syn-syn conformers are about 4 kJ/mol (E = O, S, Se) less in energy than the syn-anti conformers, whereas the energy difference for the $Te(SbMe_2)_2$ conformers is roughly 1 kJ/mol[49,50].

Even more interesting, $Te(BiEt_2)_2$ showed a very small Bi-Te-Bi bond angle of 86.606(13)°, which is well below the expected value of 90°, and an intramolecular Bi$\cdots$Bi distance of 4.0847(5) Å. Comparable findings were reported by Breunig *et al.* for the corresponding compound $[(Me_3Si)_2CH]_2Bi_2Te$ containing the sterically more demanding bis(trimethylsilyl)methyl substituents (88.00(7)°, 4.002 Å)[51]. In order to find out whether these structural findings result from weak attractive intramolecular Bi$\cdots$Bi interactions, we investigated $Te(BiR_2)_2$ (R = H, Me, and Et) along with the bismuthine dimer in detail using quantum chemical methods comprising MP2, SCS-MP2, CCSD(T) and DFT-SAPT. First, some emphasis was laid on determining the level of theory required for an appropriate theoretical description of the Bi$\cdots$Bi interactions, investigating

From DFT-SAPT calculations on the interaction of BiH_3 with the test particles He and Li^+, respectively, we also investigated the anisotropy of the various interaction energy contributions around a Bi atom embedded in a molecular environment.

METHODOLOGY

The TURBOMOLE quantum chemical program package[52,53] was used to optimize geometries and calculate vibrational frequencies. For the geometry optimizations, self-consistent field

iteration and density convergence thresholds were both lowered to 10^{-8} a.u., while the energy convergence threshold in the geometry optimization cycles was lowered to 10^{-7} a.u. and the maximum norm of the cartesian gradient to 10^{-7} a.u.. Second derivatives of the energy as required for calculation of vibrational frequencies were numerically determined from central differences employing analytical gradients with a standard differentiation increment of 0.02 a.u..

In all of our computations the Stuttgart/Cologne small-core relativistic pseudopotentials were used for Bi and Te[44,54]. While for H and C atoms standard augmented correlation consistent basis sets (aug-cc-pVXZ) with triple- (X=T), quadruple- (X=Q) and quintuple-zeta (X=5) quality[55,56] were employed, for Bi and Te in addition to their pseudopotential equivalents[57,58] also the aug-cc-pwCVXZ basis sets[59] were used to take core-valence correlation effects appropriately into account. We will denote a combination of the aug-cc-pwCVXZ basis sets for Bi and Te and aug-cc-pVXZ for C and H as awCVXZ in the following, while the aug-cc-pVXZ/aug-cc-pVXZ combination will be abbreviated as aVXZ. Note that we continue to use the same basis set labels for $Te(BiMe_2)_2$ and $Te(BiEt_2)_2$, though for these two molecules the diffuse functions on the hydrogen atoms were eliminate to improve computaational efficiency. MP2, SCS-MP2, and CCSD(T) electron correlation contributions were computed within the resolution-of-the-identitiy a.k.a. density-fitting approximation with the appropriate "MP2FIT" auxiliary basis sets[60,61]. Complete basis set (cbs) extrapolations of electron correlation contributions were carried out with the two-point X^{-3} formula of Halkier *et al.*[62], adding them to the Hartree-Fock energy as obtained with the larger of the two basis sets. All interaction energies were corrected for the basis set superposition error (BSSE) through the counterpoise correction (CPC)[63].

Density fitting DFT-SAPT computations[64] were carried out with the MOLPRO quantum chemical program[65,66], also with self-consistent field and density thresholds of 10^{-8} a.u. Numerical integrations on the exchange-correlation (xc) potential and kernel were made with grid thresholds of 10^{-8} and 10^{-6} a.u., respectively, while an eight point Gauss-Chebyshev quadrature was used for integration over the imaginary frequency as required to determine the dispersion contributions. The exchange-correlation (xc) potential for determination of the Kohn-Sham orbitals was an asymptotically corrected version of PBE0 designated as

PBE0AC[67–71], whereas response properties were computed with the help of the adiabatic local density approximation (ALDA) xc kernel[72,73]. Ionization potentials and orbital energies required for determination of the asymptotic correction were calculated for the monomers with the PBE0 xc functional and quaduple-zeta quality basis sets. Density-fitting DFT-SAPT calculations require an additional "JKFIT" auxilliary basis set besides the MP2FIT set - which unfortunately at present seems not to exist for the aug-cc-pwCVX orbital basis sets. However, in MOLPRO both kinds of auxiliary basis sets are available for the def2-ATZVPP and def2-AQZVPP orbital basis sets resulting from augmenting standard TURBOMOLE def2-TZVPP and def2-QZVPP basis sets[74] with even-tempered diffuse functions. These basis sets, in the following abbreviated as ATZVPP and AQZVPP, respectively, were thus employed along with the appropriate auxiliary basis sets in all DFT-SAPT computations.

RESULTS AND DISCUSSION

Bismuthine dimer

The aforementioned study of Moilanen *et al.*[42] on $X_3E\cdots EX_3$ (E=N, P, As, Sb, Bi; X=F, Cl, Br, I) dimers showed that (i) MP2 yields drastically too large magnitudes of the interaction energy as compared to CCSD(T) in all cases where atoms of the third and higher periods are involved, and that (ii) SCS-MP2 agrees much better with CCSD(T). However, the basis sets used in this study are not able to describe valence electron correlation effects of the d shells properly. In view of its importance in other compounds containing heavy metal atoms such as the gold atom[75] we expect correlation between the fully occupied 5d shells on the Bi atoms to be significant for interactions between them.

In order to determine the most suitable level of theory for their quantitative description thus first a set of MP2, SCS-MP2, and CCSD(T) computations was carried out on the smallest possible dimer involving Bi, i.e., $(BiH_3)_2$. Four conformers - not all of which were expected to be minima on the potential energy surface (vide infra) - were constructed in order to enable direct Bi$\cdots$Bi contacts: conformer **A** with D_{3d} symmetry, conformers **B**

and **C**, both with D_{2h} symmetry, and conformer **D** with C_i symmetry (Fig. 3). Conformer **D** differs from **C** chiefly through rotations of the BiH_3 molecules around their respective symmetry axes in opposite direction. Geometry optimizations within symmetry constraints yield very different Bi$\cdots$Bi distances depending on the electron correlation treatment and the number of correlated electrons, as shown in Table 1: comparing the MP2 and SCS-MP2 results obtained with the aVTZ and aVQZ basis sets for eight correlated electrons per BiH_3 reveals systematically shorter distances for MP2, i.e., by 0.11 - 0.18 Å, while corresponding comparisons for eighteen correlated electrons per monomer and the awCTZ and awCVQZ basis sets show even larger differences of 0.13 - 0.22 Å. The influence of including the d shells in the correlation treatment is dramatic: comparing the quadruple-zeta level results shows a shortening of the Bi$\cdots$Bi distances of 0.18 - 0.45 Å at the MP2 level and of 0.15 - 0.41 Å at the SCS-MP2 level of theory. Thus it is mandatory to include the d shells in the correlation treatment, as anticipated.

Including them and improving the basis set from quadruple- to quintuple-zeta quality yields slightly different Bi$\cdots$Bi distances, i.e., they change by up to 0.03 Å at the SCS-MP2 level (cf. Table 1). This was taken as an indication for an insufficient cancellation of basis set incompleteness (BIE) and basis set superposition (BSSE) errors with the quadruple-zeta quality basis sets and prompted us to also carry out counterpoise-corrected (CPC) geometry optimizations[76,77]. As expected, the CPC SCS-MP2 Bi$\cdots$Bi distances are all longer than their non-CPC counterparts, i.e., by about 0.03 Å with the awCVQZ basis set. Interestingly, the CPC SCS-MP2/awCVQZ Bi$\cdots$Bi bond distances agree excellently with the non-CPC SCS-MP2/awCVTZ results, i.e., within 0.005 Å. Assuming that the CPC-SCS-MP2/awCVQZ results are nearly converged with respect to basis set extension, we take this as an indication for a fairly complete cancellation between BIE and BSSE at the non-CPC SCS-MP2/awCVTZ level of theory.

For the SCS-MP2/awCVTZ optimized dimer geometries Table 2 presents counterpoise-corrected interaction energies as obtained with MP2, SCS-MP2, and CCSD(T) for eighteen correlated electrons per BiH_3 and quintuple-zeta quality basis sets, demonstrating that MP2 overbinds as compared to the "gold standard" CCSD(T) by as much as 1.8 - 2.8 kJ/mol, while SCS-MP2 agrees with CCSD(T) within about 0.3 kJ/mol. Thus SCS-MP2 is expected to

provide a reasonable approximation to CCSD(T) for the purpose of geometry optimization. Furthermore, in view of the large number of electrons (98) to be included in a correlation treatment of $Te(BiEt_2)_2$ the basis set should be kept as small as possible. All in all, the non-CPC SCS-MP2/awCVTZ level of theory thus appears to be a reasonable compromise between accuracy and efficiency.

Table 2 also contains the results of a complete basis set (cbs) extrapolation employing quadruple- and quintuple-zeta CP-corrected correlation energies which were added to the CP-corrected quintuple-zeta Hartree-Fock interaction energies, yielding CCSD(T)/cbs estimates of -2.17, -4.86, -7.59, and -8.57 kJ/mol of the interaction energies of structures **A**, **B**, **C**, and **D** respectively. These estimates are likely to be accurate within a few hundredths of a kJ/mol, as shown by comparison to corresponding estimates using triple- and quadruple basis sets (Table S1, Supplementary Information (SI)). However, it should be noted that none of the structures **A**, **B**, and **C** represents a stable conformer of $(BiH_3)_2$: harmonic vibrational frequency determinations carried out with SCS-MP2/awCVTZ reveal a total of five negative curvatures for structures **A**, and two for both, structures **B**, and **C**. Structure **D**, on the other hand, is found to be a stable conformer.

While the large differences between the interaction energies as obtained from Hartree-Fock, which are all positive, and those of the various electron-correlation methods (cf. Table 2) already indicate at the dispersion-dominance of the Bi$\cdots$Bi interactions, this can be directly proven through DFT-SAPT. Table 3 shows the individual DFT-SAPT interaction energy contributions as obtained with a quadruple-zeta quality basis set, which in Figure 4 are grouped as $E_{\rm el} = E_{\rm el}^{(1)}$, $E_{\rm exch} = E_{\rm exch}^{(1)}$, $E_{\rm IND} = E_{\rm ind}^{(2)} + E_{\rm exch-ind}^{(2)} + \delta({\rm HF})$, and $E_{\rm DISP} = E_{\rm disp}^{(2)} + E_{\rm exch-disp}^{(2)}$. A glance at the figure immediately shows that the dispersion contribution $E_{\rm DISP}$ is dominant in all four structures. Though the electrostatic contribution $E_{\rm el}$ clearly contributes less to the attraction between the monomers, it may nevertheless be seen as influencing the relative stabilities of the three structures, as $E_{\rm DISP}$ and the exchange a.k.a. exchange-overlap contribution $E_{\rm exch}$ representing "steric repulsion" cancel for the most part in each case. Interestingly, the total induction energies $E_{\rm IND}$ are relatively unimportant, with the exception of structure **A**, where it becomes repulsive. This is due to differing signs of the second-order contributions $E_{\rm ind}^{(2)} + E_{\rm exch-ind}^{(2)}$ on the one hand and of the δ(HF) estimate[78,79] of the higher-

order induction plus exchange-induction energies on the other hand (cf. Table 3). It should be noted that the latter is a Hartree-Fock level estimate only, and since it is a sizeable contribution, in particular in the case of structures **A** and **D**, it may significantly contribute to the deviations of 0.4 - 0.8 kJ/mol of the cbs-extrapolated DFT-SAPT interaction energies (cf. Table 3) from their CCSD(T) counterparts (cf. Table 2). There is a list of further possible reasons for deviations between DFT-SAPT and CCSD(T), of course, including: (i) neglect of third and higher order dispersion and induction dispersion contributions in SAPT[80], (ii) the quality of the xc potential and kernel used in DFT-SAPT[71,81–83], (iii) approximations as concerning the exchange contributions inherent in DFT-SAPT[84], (iv) the perturbative approximation of the triple excitation contribution and the neglect of higher excitations in CCSD(T)[85], and (v) uncertainties of the cbs extrapolation scheme, which in case of DFT-SAPT for technical reasons (vide supra) was based on dispersion and exchange-dispersion contributions as obtained with ATZVPP (Table S2, SI) and AQZVPP basis sets instead of with augmented correlation-consistent basis sets, the latter providing a much better tested platform for this purpose. Nevertheless, with the exception of structure **A**, the cbs extrapolated interaction energies agree within better than 10%, as usually also observed for molecular dimers consisting of only light atoms[36].

Anisotropy of interactions with bismuthine

While the Bi$\cdots$Bi distance in structures **A** and **B** of $(BiH_3)_2$ is close to 4.7 Å, in structure **C** it is reduced by more than 0.3 Å to 4.36 Å. This is still considerably longer than the 4.085 Å experimentally observed[45] for the intramolecular Bi$\cdots$Bi distance in $Te(BiEt_2)_2$, raising the question of the anisotropy of interactions with Bi atoms in a molecular environment.

Two model systems were investigated to approach this question with the help of DFT-SAPT computations: He$\cdots$$BiH_3$ and $Li^+\cdots BiH_3$, with He and Li^+ serving as test particles for mapping the size of the various interaction energy contributions as a function of the distance of the test particle from the Bi atom and its angle with the symmetry axis (cf. Fig. 5). Similar ineraction energy contribution maps based on SAPT have already been used before, e.g., using a point charge for the induction contribution[86] or a neon atom for the

dispersion contribution[87]. Exchange and dispersion "predisposition maps" obtained from He$\cdots$BiH$_3$ by moving the test particle in the C$_s$-plane of BiH$_3$ are shown as contour plots in Figure 6. The mild variations of E_{DISP} for angles of -80° to +60° between the C_{3v} axis and the Bi$\cdots$He line, i.e., the area around the exposed Bi atom, confirm common wisdom on the isotropy of dispersion interactions. Clearly, this is not true for the exchange contribution E_{exch}, which is much more repulsive along the symmetry axis than in the regions orthogonal to it, where it can be said to exhibit "holes". The resulting sum of the dispersion and steric repulsion energies - which may be termed "van der Waals-interaction energy" - is strongly anisotropic: its "zero-line" (Fig. 6c) clearly shows that interaction partners may get much closer to the Bi atom when they approach BiH$_3$ "from the side", i.e., with angles to the symmetry axis of about +60° and -80°, respectively. The corresponding angles between the Bi atom of one molecule and the symmetry axis of the other monomer in structures **B** and **C** of (BiH$_3$)$_2$ are about +80° and -100°, respectively, suggesting that the Bi$\cdots$Bi distances in both cases are not as small as they "optimally" could be if there were only van der Waals interactions between the Bi atoms, as is obviously not the case.

Besides the presence of the hydrogen atoms, clearly visible in Fig. 6 through the increase of the magnitude of both, E_{exch} and E_{DISP} around +125° and -150°, one can also not ignore the electrostatic and induction contributions, which are more sensibly mapped with a charged test particle. Corresponding predisposition maps as obtained from Li$^+\cdots$BiH$_3$ are shown in Figure 7. The map of E_{el} mainly reflects the fact that despite the small electronegativity difference between Bi and H atoms there is a non-zero dipole moment for BiH$_3$ of (1.17 Debye with SCS-MP2/acwVTZ, and 1.02 Debye with PBE0/acwVTZ at the SCS-MP2/acwVTZ geometry), corresponding to a positive partial charge on Bi and compensating negative partial charges on the H atoms. An interaction with a positively charged ion thus is expected to be repulsive (blue contour lines) around the Bi atom, and attractive (red contour lines) at the hydrogen end of the molecule, and crosses through zero (green contour line) at angles of about ±90°. Interestingly, the largest electrostatic repulsion is not observed for an angle of 0°, i.e., on top of Bi along the symmetry axis, but rather at angles of -45° to -60°, somewhat reduced at angles around +45°. The induction predisposition map, on the other hand, resembles the dispersion predisposition map shown above.

The interaction energy contribution predisposition maps help to rationalize relative energies and structural parameters of the various $(BiH_3)_2$ dimers: **C** is the most stable of the considered symmetrical structures since (i) two negatively charged H atoms may come in close contact with each Bi atom, leading to significant electrostatic stabilization, and, more importantly, (ii) the hole in the exchange contribution for the resulting orientation of the two anisotropic Bi atoms allows for a strong dispersion stabilization and thus for relatively small Bi$\cdots$Bi distances, until the dispersion contribution is essentially compensated by the exchange contribution (cf. Fig. 4) which exponentially increases with decreasing distance. While for structure **B** there must be a smaller amount of electrostatic stabilization, since here only one H atom is in close contact with each Bi, the smaller hole in the exchange contribution for the resulting orientation of the two anisotropic Bi atoms keeps them further apart, leading to a reduction of the size of all interaction energy contributions. Finally, for structure **A** in a naive picture the two positively charged Bi atoms should repel each other. The DFT-SAPT computations for the dimer in this structure nevertheless show an overall attractive electrostatic contribution (cf. Fig. 4), as in nearly all close-contact cases: the attraction between the nuclei of one molecule and the electron distribution of the other usually overcompensates the repulsion between the respective nuclei and electron distributions. Nevertheles, attraction between the two monomers in this orientation is mainly due to the dispersion contribution, attempting to bring the two Bi atoms in the closest possible contact until the exponential exchange contribution significantly sets in, which is the case for relatively large distances from the Bi atom for an approach along the symmetry axis (cf. Fig. 6).

Structures and energetics of $Te(BiR_2)_2$

In a system like $Te(BiH_2)_2$ with a presumed Bi-Te-Bi angle of around 90° the second Bi atom approaches the first Bi atom at an angle of about +80° with a formal "symmetry axis", the latter constructed from replacing the Bi-Te bond with a Bi-H bond. This angle coincides with the corresponding angle in structure **B** of $(BiH_3)_2$, so that at first sight a similar Bi$\cdots$Bi distance of about 4.7 Å could be expected. However, the situation is different in $Te(BiH_2)_2$:

now both Bi atoms are covalently linked to the same atom such that there is no longer a steric repulsion from an H atom acting on the neighboring Bi atom as in $(BiH_3)_2$.

SCS-MP2/awCVTZ geometry optimizations on $Te(BiH_2)_2$ yield two stable monomer structures (Fig. 8): a C_1-symmetrical syn-anti conformer and a C_{2v}-symmetrical syn-syn conformer which is higher in energy by 2.34 kJ/mol. Adding zero point vibrational energies (ZPVE) in the harmonic approximation results in a slight increase of the energy difference to 2.40 kJ/mol. Neglecting vibrational corrections the barrier of interconversion between the conformers is inferred as about 6.5 kJ/mol through scanning along a single Bi-Te-Bi-H torsion angle (optimizing all remaining structural parameters), i.e., it amounts to only about half of the rotation barrier in ethane. The Bi$\cdots$Bi distance is shortest for the syn-syn conformer in which it amounts to 4.015 Å, and it increases to 4.030 Å in the approximate transition state, which was taken as the structure with the highest energy and the smallest gradient along the Bi-Te-Bi-H torsion angle scan (Table S3, SI). With 4.040 Å the Bi$\cdots$Bi distance is longest in the syn-anti conformer in which the two hydrogen atoms pointing "inwards" apparently exert a slight sterical repulsion on the neighboring Bi atom. On the other hand, this arrangement certainly maximizes dispersion and eletrostatic interactions between the two BiH_2 groups, which might also contribute to the breaking away from C_s symmetry in the syn-anti conformer through bringing one of the hydrogen atoms of one BiH_2 group closer to the atoms of the other BiH_2 group. A C_s-symmetrized form of the syn-anti conformer was found to be 0.54 kJ/mol higher in energy than the C_1-symmetrical minimum conformation, it represents a first-order saddle point on the potential energy surface. The Bi-Te-Bi angle is nearly independent on the considered structure, i.e., it is calculated as 90.12° for the syn-syn conformer, 90.23° for the transition state, and 90.88° for the syn-anti conformer.

For $Te(BiMe_2)_2$ the SCS-MP2/awCVTZ geometry optimizations also result in two stable conformers (Fig. 9), a syn-anti conformer with C_1 and a syn-syn conformer with C_{2v} symmetry. The latter again is higher in energy, but only by 0.10 kJ/mol, which slightly increases to 0.16 kJ/mol after correction for zero point vibrations. Defining, as already for $Te(BiH_2)_2$, the interconversion barrier as the energy difference between the transition state and the lower of the two stable conformers, with 5.7 kJ/mol (Table S4, SI) is found to be even smaller than that of $Te(BiH_2)_2$. The Bi$\cdots$Bi distance in the syn-syn conformer with

4.059 Å is somewhat longer than that in the corresponding conformer of $Te(BiH_2)_2$, and the Bi-Te-Bi angle with 91.59° accordingly larger. In the syn-anti conformer, on the other hand, one observes a drastic increase of the Bi···Bi distance to 4.236 Å and of the Bi-Te-Bi angle to 96.75°, a clear indication for steric repulsion between the methyl groups pointing inwards and the neighboring Bi atom. Though this close contact situation should also lead to larger attractive dispersion interactions between the $BiMe_2$ groups in the syn-anti conformer as compared to the syn-syn conformer, in the former the increased repulsive exchange-overlap interactions dominate, lifting its energy relative to that of the syn-syn conformer, which does not suffer from steric repulsion.

Starting from the geometry of a $Te(BiEt_2)_2$ molecule as found in the crystal SCS-MP2/awCVTZ geometry optimizations led to a C_2-symmetrical syn-syn conformer. This, however, is 0.12 kJ/mol higher in energy than a C_1-symmetrical form of the syn-syn conformer in which one of the $BiEt_2$ groups is somewhat rotated around the Te-Bi bond, bringing one of its ethyl groups closer to the Bi atom and an ethyl group of the other $BiEt_2$, which maximizes their dispersion interactions (Fig. 10). The Bi···Bi distance in this conformer is 4.017 Å, the Bi-Te-Bi angle 90.33°. Scanning a Bi-Te-Bi-C angle (Table S5, SI) one reaches a C_1-symmetrical syn-anti conformer over the top of a 7.2 kJ/mol high barrier. In contrast to $Te(BiH_2)_2$ and $Te(BiMe_2)_2$ the syn-anti conformer of $Te(BiEt_2)_2$ is higher in energy than its syn-syn counterpart, by 0.86 kJ/mol before and by 1.18 kJ/mol after zero point vibrational energy correction. The Bi···Bi distance in the syn-anti conformer is as long as 4.342 Å, with an according Bi-Te-Bi angle of 99.96°, clearly resulting from the higher sterical demand of the ethyl groups compared to the methyl groups of $Te(BiMe_2)_2$. Fixing the Bi-Te-Bi-C torsion angle to the value of 173.8° as found in the crystal structure and optimizing all other geometry parameters under C_2 symmetry constraints raises the energy by 2.25 kJ/mol, but changes the Bi···Bi distance with 4.036 Å and the Bi-Te-Bi angle with 90.7° only slightly as compared to the same structural parameters in the C_1-symmetrical syn-syn conformer. In the crystal structure there are additional intermolecular Bi···Te contacts with distances of 3.389 Å, which help to stabilize a somewhat "twisted" monomer.

It should be noted that for the syn-syn conformers of all of the studied $Te(BiR_2)_2$ systems the calculated Bi···Bi distances are even slightly shorter (by 0.03 to 0.07 Å) than the crystal

structure value of 4.085 Å for $Te(BiEt_2)_2$, while the calculated Bi-Te-Bi angles are 4 to 5° larger than observed in the crystal structure (86.61°). This seeming contradiction is resolved by noting that the Te-Bi bond distances as determined with SCS-MP2 are by 0.141 to 0.147 Å shorter than the crystal structure value of 2.978 Å for $Te(BiR_2)_2$. Fixing the Te-Bi distance to this number and optimizing all other structural parameters of the C_{2v}-symmetrical syn-syn conformers of $Te(BiH_2)_2$ and $Te(BiMe_2)_2$ with SCS-MP2/awCVTZ leads to a Bi$\cdots$Bi distances of 4.155 and 4.182 Å, respectively, and to Bi-Te-Bi angle of 88.48° and 89.19°, showing that angles below 90° should result from quantum chemical methods which (i) correctly describe the interatomic electron correlation a.k.a. dispersion interactions between the neighboring Bi atoms, as indeed has been shown to be the case for SCS-MP2 when correlating the electrons in the d shells, and (ii) at the same time get the Te-Bi bond length more accurately than SCS-MP2. While CCSD(T) is the best candidate to fulfill both criteria it is also computationally challenging. It remains to be seen which of the numerous dispersion-corrected DFT-based approaches provides a feasible way out of this dilemma.

CONCLUSIONS

Our calculations on the bismuthine dimer geometries and interaction energies have shown that it is mandatory to include the electrons in the d shells of the heavy atoms in supermolecular wavefunction-based electron correlation methods as MP2, SCS-MP2 and CCSD(T). Taking the counterpoise correction and complete basis set extrapolation into account our results confirm that MP2 drastically overestimates the magnitude of the interaction energy for dimer structures with close Bi$\cdots$Bi contacts as compared to the CCSD(T) reference, while SCS-MP2 performs quite well in this respect. The dispersion-dominance of the interactions was proven with the help of DFT-SAPT computations on the same set of $(BiH_3)_2$ structures. While the total DFT-SAPT interaction energy deviates significantly from CCSD(T) for the most weakly interacting structure **A**, which might be due to inaccuracies in the estimate of the relatively sizeable third- and higher-order induction and exchange-induction effects, for structures **B**, **C**, and **D** the agreement between DFT-SAPT and CCSD(T) is about as good as for dimeric systems which consist of light atoms only. CBS-extrapolated DFT-SAPT and

CCSD(T=) interaction energies for the stable conformer **D** of $(BiH_3)_2$ were determined as -9.36 and -8.57 kJ/mol, respectively.

Dispersion and exchange predisposition maps generated form DFT-SAPT calculations for the interaction of BiH_3 with a He atom as test particle show that the dispersion contribution is fairly isotropic around the exposed Bi atom, while the exchange-overlap contribution is not. The latter, representing steric repulsion at short interatomic distances, displays a "hole" region at angles of around 90° with the symmetry axis of BiH_3, meaning that an interaction partner may more closely approach the Bi atom "from the side" than "from above". In combination with an electrostatic interaction energy map generated using Li^+ this allowed to rationalize the calculated trends of Bi$\cdots$Bi distances and interaction energies for the investigated D_{3d}- and C_{2h}-symmetrical structures of $(BiH_3)_2$, none of which represents a local minimum on the dimer potential energy surface. We hope that interaction energy predisposition maps will turn out as useful tools for qualitative predictions of minima on the potential energy surface of interacting molecules as well.

In the $Te(BiR_2)_2$ molecules (R=H, Me, Et) the Bi atoms in the two BiR_2 groups approach each other "from the side", yet in contrast to structures **B** and **C** of $(BiH_3)_2$ without any sterical hindrance from a close-contact hydrogen atom, thus allowing even shorter distances between the Bi atoms attracting each other through dispersion interactions. For the syn-syn conformers the intramolecular Bi$\cdots$Bi distances vary between 4.015 and 4.059 Å according to SCS-MP2 geometry optimizations which take correlation of the d electrons into account. While they thus are even slightly shorter (by 0.03 - 0.07 Å) than the measured distance in the crystal of $Te(BiEt_2)_2$, the calculated Bi-Te-Bi angles are all larger (by 4 to 5°) than the experimental value of 86.6°, which was traced back to a significant underestimation (by 0.14 -0.15 Å) of the length of the Te-Bi by SCS-MP2. It is a serious challenge for quantum chemical approaches to get the subtle interplay between covalent and noncovalent forces present in the $Te(BiRt_2)_2$ right, suggesting them as benchmark systems in the heavy atom regime.

Finally, the complex interplay between dispersion attraction and steric repulsion between the neighboring Bi atoms and their ligands leads to a clear trend in the relative stability of the syn-syn and syn-anti conformers of the $Te(BiR_2)_2$ molecules: while in $Te(BiH_2)_2$ the syn-anti

conformer is more stable than the syn-syn conformer (by 2.4 kJ/mol after ZPVE correction), the two confomers are predicted to be nearly isoenergetic in $Te(BiMe_2)_2$ (within 0.2 kJ/mol), and finally the syn-syn conformer becomes the more stable conformer in $Te(BiEt_2)_2$ (by 1.2 kJ/mol) - in nice agreement with expectations based on the sterical demand of the ligands, which point "inwards" for the syn-anti conformers. Still, these energy differences are so small that both conformers are to be expected in the gas phase. Their experimental detection, however, will require low-temperature techniques, as the interconversion barriers range from 5.7 ($Te(BiMe_2)_2$) over 6.5 ($Te(BiH_2)_2$) to 7.2 kJ/mol ($Te(BiEt_2)_2$) only.

ACKNOWLEDGMENTS

We are grateful for financial support of this work in the framework of the priority program SPP 1807 "Control of London Dispersion Interactions in Molecular Chemistry" of the Deutsche Forschungsgemeinschaft (DFG), grant numbers SCHU1069/19-1 and JA954/4-1.

(Additional Supporting Information (SI) may be found in the online version of this article.)

References

1. P. R. Schreiner, L. V. Chernish, P. A. Gunchenko, E. Y. Tikhonchuk, H. Hausmann, M. Serafin, S. Schlecht, J. E. P. Dahl, R. M. K. Carlson, A. A. Fokin, Nature, **2011**, 477, 308.

2. D. J. Liptrot, P. P. Power, Nat. Rev., **2017**, 1, 0004.

3. B. D. Rekken, T. M. Brown, J. C. Fettinger, F. Lips, H. M. Tuononen, R. H. Herber, P. P. Power, J. Am. Chem. Soc., **2013**, 135, 10134.

4. J.-D. Guo, D. J. Liptrot, S. Nagase, P. P. Power, Chem. Sci., **2015**, 6, 6235.

5. F. Scherbaum, A. Grohmann, B. Huber, C. Krüger and H. Schmidbaur, Angew. Chem. Int. Ed. Engl., **1988**, 27, 1544.

6. P. Pyykkö, Chem. Rev., **1997**, 97, 597.

7. P. Pyykkö, Angew. Chem. Int. Ed., **2004**, 43, 4412.

8. P. Pyykkö, Inorg. Chim. Acta, **2005**, 358, 4113.

9. P. Pyykkö, Chem. Soc. Rev., **2008**, 37, 1967.

10. H. Schmidbaur and A. Schier, Chem. Soc. Rev., **2008**, 37, 1931.

11. M. Mantina, A. C. Chamberlin, R. Valero, C. J. Cramer, D. G. Truhlar, J. Phys. Chem. A, **2009**, 113, 5806.

12. A. J. Ashe, III, E. G. Ludwig, Jr., J. Oleksyszyn, J. C. Huffman, Organometallics, **1984**, 3, 337.

13. A. Kuczkowski, S. Heimann, A. Weber, S. Schulz, D. Bläser, C. Wölper, Organometallics, **2011**, 30, 4730.

14. S. Schulz, S. Heimann, A. Kuczkowski, C. Wölper, D. Bläser, Organometallics, **2013**, 32, 3391.

15. H. J. Breunig, H. Jawad, J. Organomet. Chem., **1984**, 277, 257.

16. H. J. Breunig, K. H. Ebert, R. E. Schulz, M. Wieber, I. Sauer, Z. Naturforsch., **1995**, 50b, 735.

17. H. J. Breunig, L. Königsmann, E. Lork, M. Nema, N. Philipp, C. Silvestru, A. Soran, R. A. Varga, R. Wagner, Dalton Trans., **2008**, 1831.

18. H.J. Breunig, S. Gülec, Z. Naturforsch. B, **1986**, 41, 1387.

19. R. S. Dickson, K. D. Heazle, J. Organomet. Chem., **1995**, 493, 189.

20. M. Wieber, I. Sauer, Z. Naturforsch. B, **1984**, 39, 1668.

21. H. J. Breunig, W. W. du Mont, D. Müller, T. Severengiz, Z. Naturforsch. B, **1985**, 40, 848.

22. A. J. Ashe, III, E. G. Ludwig, Jr., J. Organomet. Chem., **1986**, 308, 289.

23. F. Calderazzo, A. Morvillo, G. Pelizzi, R. Poli, F. Ungari, Inorg. Chem., **1988**, 27, 3730.

24. H.J. Breunig, S. Gülec, In *Unkonventionelle Wechselwirkungen in der Chemie metallischer Elemente*, B. Krebs (Ed.), VCH, Weinheim, 1992, 218.

25. T. Hughbanks, R. Hoffmann, M.-H. Whangbo, K. R. Stewart, O. Eisenstein, E. Canadell, J. Am. Chem. Soc., **1982**, 104, 3876.

26. K. Klinkhammer, P. Pyykkö, Inorg. Chem., **1995**, 34, 4134.

27. H. Bürger, R. Eujen, G. Becker, O. Mundt, M. Westerhausen, C. Witthauer, J. Mol. Struct., **1983**, 98, 265.

28. M. Hartmann, L. Radom, J. Phys. Chem. A, **2**000, 104, 968.

29. S. Ishida, F. Hirakawa, K. Furukawa, K. Yoza,, T. Iwamoto, Angew. Chem. Int. Ed., **2014**, 53, 11172.

30. J.-D. Guo, S. Nagase, P. P. Power, Organometallics, **2015**, 34, 2028.

31. S. Grimme, WIREs Comput. Mol. Sci., **2011**, 1, 211.

32. K. Pernal, R. Podeszwa, K. Patkowski, K. Szalewicz, Phys. Rev. Lett., **2009**, 103, 263201.

33. B. Jeziorski, R. Moszynski, K. Szalewicz, Chem. Rev., **1994**, 94, 1887.

34. K. Szalewicz, K. Patkowski, B. Jeziorski, Struct. Bond., **2005**, 116, 43.

35. K. Szalewicz, WIREs Comput. Mol. Sci., **2012**, 2, 254.

36. G. Jansen, WIREs Comput. Mol. Sci., **2014**, 4, 127.

37. M. Modrzejewski, L. Rajchel, M. Szczesniak, G. Chałasinski, J. Chem. Phys., **2012**, 136, 204109.

38. R.-F. Liu, C. A. Franzese, R. Malek, P. S. Zuchowski, J. G. Ángyán, M. M. Szczesniak and G. Chałasinski, J. Chem. Theor. Comput., **2011**, 7, 2399.

39. J. Muñiz, C. Wang, P. Pyykkö, Chem. Eur. J., **2011**, 17, 368.

40. R. Lo, P. Svec, Z. Ruzickova, A. Ruzicka, P. Hobza, Chem. Commun., **2016**, 52, 3500.

41. A. A. Auer, D. Mansfeld, C. Nolde, W. Schneider, M. Schürmann, M. Mehring, Organometallics, **2009**, 28, 5405.

42. J. Moilanen, C. Ganesamoorthy, M. S. Balakrishna, H. M. Tuononen, Inorg. Chem., **2009**, 48, 6740.

43. S. Grimme, J. Chem. Phys., **2003**, 118, 9095.

44. X. Cao, M. Dolg, WIREs Comput. Mol. Sci., **2011**, 1, 200.

45. S. Heimann, A. Kuczkowski, D. Bläser, C. Wölper, R. Haack, G. Jansen, S. Schulz, Eur. J. Inorg. Chem., **2014**, 4858.

46. S. Heimann, S. Schulz, D. Bläser, C. Wölper, Eur. J. Inorg. Chem., **2013**, 4909.

47. S. Heimann, D. Bläser, C. Wölper, S. Schulz, Organometallics, **2014**, 33, 2295.

48. H. J. Breunig, E. Lork, R. Rösler, G. Becker, O. Mundt, W. Schwarz, Z. Anorg. Allg. Chem., **2000**, 626, 1595.

49. A. Haaland, V. I. Sokolov, H. V. Volden, H. J. Breunig, M. Denker, R. Rösler, Z. Naturforsch. B, **1997**, 52, 296.

50. A. Haaland, D. J. Shorokhov, H. V. Volden, H. J. Breunig, M. Denker, R. Rösler, Z. Naturforsch. B, **1998**, 53, 381.

51. H. J. Breunig, I. Ghesner, E. J. Lork, J. Organomet. Chem., **2002**, 664, 130.

52. TURBOMOLE V7.1, 2016, a development of University of Karlsruhe and Forschungszentrum Karlsruhe GmbH, 1989-2007, TURBOMOLE GmbH, since 2007; available from http://www.turbomole.com.

53. F. Furche, R. Ahlrichs, C. Hättig, W. Klopper, M. Sierka, F. Weigend, WIREs Comput. Mol. Sci., **2014**, 4, 91.

54. B. Metz, H. Stoll, M. Dolg, J. Chem. Phys., **2000**, 113, 2563.

55. T. H. Dunning, Jr., J. Chem. Phys., **1989**, 90, 1007.

56. R. A. Kendall,T. H. Dunning, Jr., R. H. Harrison, J. Chem. Phys., **1992**, 96, 6796.

57. K. A. Peterson, J. Chem. Phys., **2003**, 119, 11099.

58. K. A. Peterson, D. Figgen, E. Goll, H. Stoll, M. Dolg, J. Chem. Phys., **2003**, 119, 11113.

59. K.A. Peterson, K.E. Yousaf, J. Chem. Phys., **2010**, 133, 174116.

60. F. Weigend, A. Köhn and C. Hättig, J. Chem. Phys., **2002**, 116, 3175.

61. C. Hättig, G. Schmitz, J. Koßmann, Phys. Chem. Chem. Phys., **2012**, 14, 6549.

62. A. Halkier, T. Helgaker, P. Jørgensen, W. Klopper, H. Koch, J. Olsen, A. K. Wilson, Chem. Phys. Lett., **1998**, 286, 243.

63. S. F. Boys, F. Bernardi, Mol. Phys., **1970**, 19, 553.

64. A. Heßelmann, G. Jansen, M. Schütz, J. Chem. Phys., **2005**, 122, 014103.

65. MOLPRO, version 2010.1, a package of ab initio programs, H.-J. Werner, P. J. Knowles, G. Knizia, F. R. Manby, M. Schütz, P. Celani, T. Korona, R. Lindh, A. Mitrushenkov, G. Rauhut, K. R. Shamasundar, T. B. Adler, R. D. Amos, A. Bernhardsson, A. Berning, D. L. Cooper, M. J. O. Deegan, A. J. Dobbyn, F. Eckert, E. Goll, C. Hampel, A. Hesselmann, G. Hetzer, T. Hrenar, G. Jansen, C. Köppl, Y. Liu, A. W. Lloyd, R. A. Mata, A. J. May, S. J. McNicholas, W. Meyer, M. E. Mura, A. Nicklass, D. P. ONeill, P. Palmieri, K. Pflüger, R. Pitzer, M. Reiher, T. Shiozaki, H. Stoll, A. J. Stone, R. Tarroni, T. Thorsteinsson, M. Wang, A. Wolf, see http://www.molpro.net.

66. H.-J. Werner, P. J. Knowles, G. Knizia, F. R. Manby, M. Schütz, WIREs Comput. Mol. Sci., **2012**, 2, 242.

67. J. P. Perdew, K. Burke, and M. Ernzerhof, Phys. Rev. Lett., **1996**, 77, 3865.

68. C. Adamo, V. Barone, J. Chem. Phys., **1999**, 110, 6158.

69. R. van Leeuwen, E. J. Baerends, Phys. Rev. A, **1994**, 49, 2421.

70. M. Grüning, O. V. Gritsenko, S. J. A. van Gisbergen, E. J. Baerends, J. Chem. Phys., **2001**, 114, 652.

71. A. Heßelmann, G. Jansen, Chem. Phys. Lett., **2002**, 357, 464.

72. E. K. U. Gross, J. F. Dobson and M. Petersilka, Top. Curr. Chem., **1996**, 181, 81.

73. A. Heßelmann, G. Jansen, Phys. Chem. Phys., **2003**, 5, 5010.

74. F. Weigend, R. Ahlrichs, Phys. Chem. Chem. Phys.. **2005**, 7, 3297.

75. P. Pyykkö, N. Runeberg, F. Mendizabal, Chem. Eur. J., **1997**, 3, 1451.

76. S. S. Xantheas, J. Chem. Phys., **1996**, 104 , 8821.

77. S. Simon, M. Duran and J. J. Dannenberg, J. Chem. Phys., **1996**, 105, 11024.

78. M. Jeziorska, B. Jeziorski, K. Cizek, Int. J. Quantum Chem., **1987**, 32, 149.

79. R. Moszynski, T. G. A. Heijmen, B. Jeziorski, Mol. Phys., **1996**, 88, 741.

80. K. Patkowski, K. Szalewicz, B. Jeziorski, J. Chem. Phys., **2006**, 125, 154107.

81. A. Misquitta, K. Szalewicz, Chem. Phys. Lett., **2002**, 357, 301.

82. A. Misquitta, K. Szalewicz, J. Chem. Phys., **2005**, 122, 214109.

83. T. Korona, Mol. Phys., **2013**, 111, 3705.

84. G. Jansen, A. Heßelmann, J. Phys. Chem. A, **2001**, 105, 11156.

85. M. Rode, J. Sadlej, R. Moszynski, P. E. S. Wormer, A. van der Avoird, Chem. Phys. Lett., **1999**, 314, 326.

86. A.J. Misquitta, A.J. Stone, S.L. Price, J. Chem. Theory Comput., **2008**, 4, 19.

87. A.J. Misquitta, A.J. Stone, Mol. Phys., **2**008, 106, 1631.

Figure 1: Typical metal$\cdots$metal interactions in solid state structures of distibines and dibismuthines.

Figure 2: Syn-syn conformer of $Te(SbMe_2)_2$ (a), syn-anti conformer of $Te(SbEt_2)_2$ (b), and syn-syn conformer of $Te(BiEt_2)_2$ (c), as observed in the solid state structures[46,47].

Figure 3: SCS-MP2/awCVTZ optimized structures of $(BiH_3)_2$.

Figure 4: DFT-SAPT/AQZVPP interaction energy contributions for the computed structures of $(BiH_3)_2$.

Figure 5: Coordinate system for the generation of the interaction energy contribution predisposition maps from DFT-SAPT/AQZVPP computations for He$\cdots$$BiH_3$ (analogous coordinates used for $Li^+\cdots BiH_3$).

Figure 6: Predisposition maps from He$\cdots$$BiH_3$ for the exchange (a, contour levels starting at +0.26 kJ/mol for large R and linearly varying up to +2.6 kJ/mol) and dispersion contributions (b, contour levels starting at -0.26 kJ/mol for large R and linearly varying down to -2.6 kJ/mol) and their sum (c, only contour level at $\pm$0 kJ/mol shown).

Figure 7: Predisposition maps from $Li^+\cdots BiH_3$ for the electrostatic (a, contour lines varying in intervals of +2.6 kJ/mol; green: $\pm$ 0 kJ/mol; blue: positive values; red: negative values) and induction contributions (b, contour levels starting at -5.2 kJ/mol for large R and linearly varying down to -26 kJ/mol).

Figure 8: Calculated gas phase conformers of $Te(BiH_2)_2$ (l.h.s.: syn-syn conformer, r.h.s.: syn-anti conformer) and transition state between them.

Figure 9: Calculated gas phase conformers of $Te(BiMe_2)_2$ (l.h.s.: syn-syn conormer, r.h.s.: syn-anti conformer) and transition state between them.

Figure 10: Calculated structures of $Te(BiEt_2)_2$. From the left to the right: C_2-symmetrical structure with Bi-Te-Bi-C torsion angle fixed to 173.8^o (see text), syn-syn conformer, transition state, syn-anti conformer.

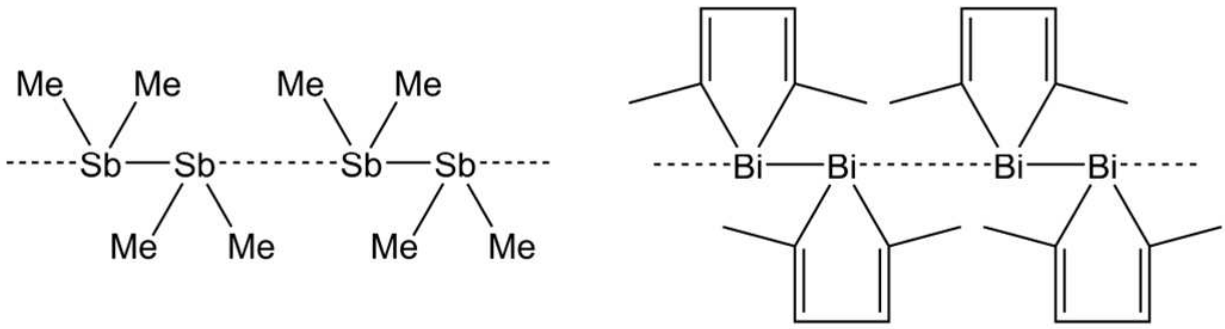

Figure 1
Georg Jansen, Stephan Schulz
J. Comput. Chem.

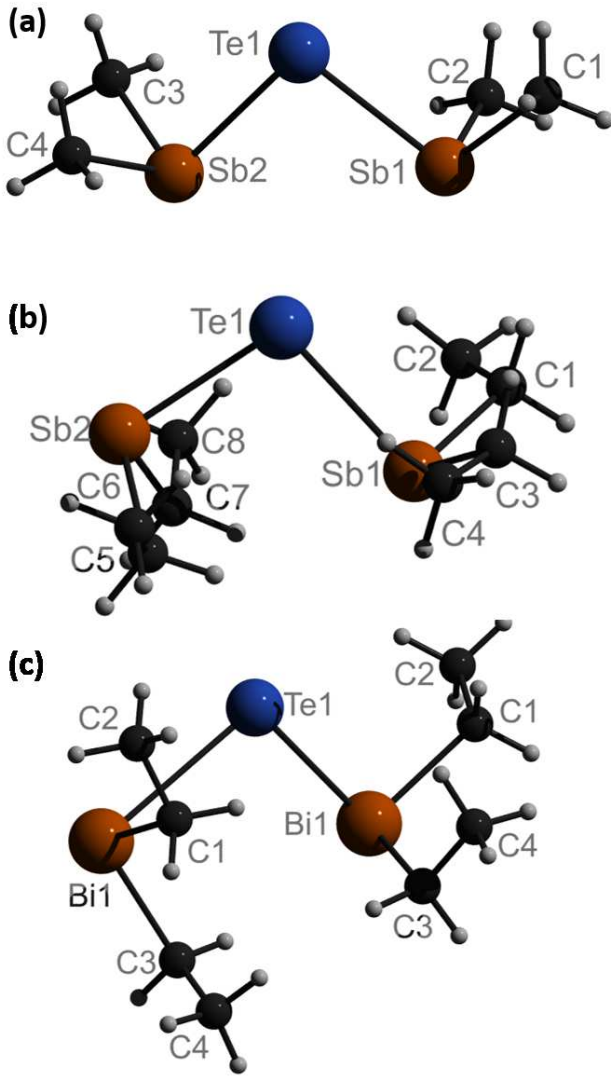

Figure 2
Georg Jansen, Stephan Schulz
J. Comput. Chem.

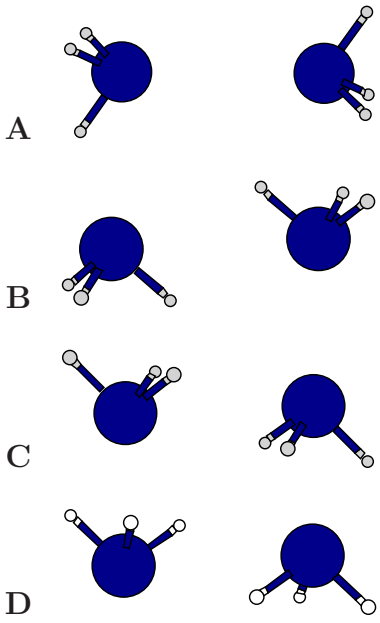

Figure 3
Georg Jansen, Stephan Schulz
J. Comput. Chem.

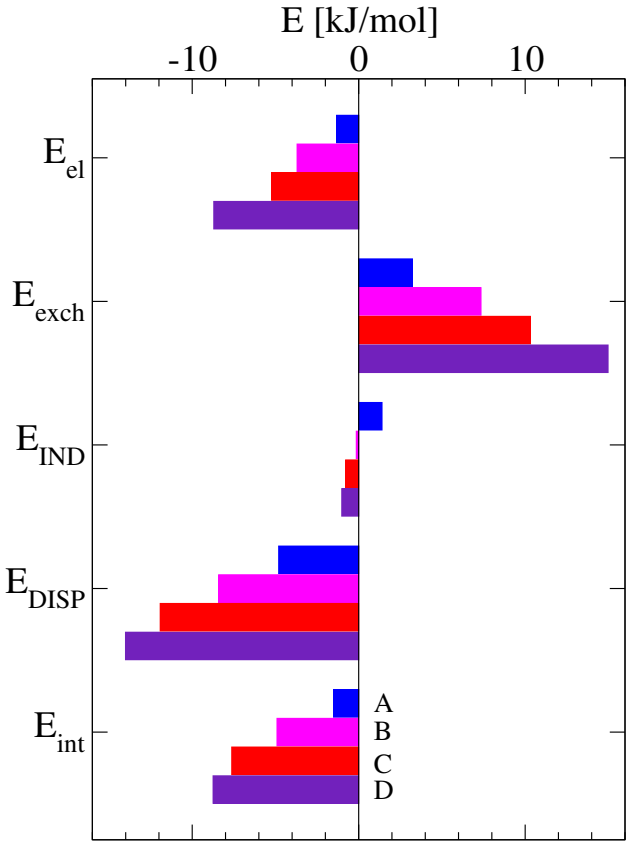

Figure 4
Georg Jansen, Stephan Schulz
J. Comput. Chem.

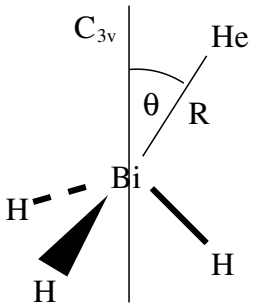

Figure 5
Georg Jansen, Stephan Schulz
J. Comput. Chem.

(a)

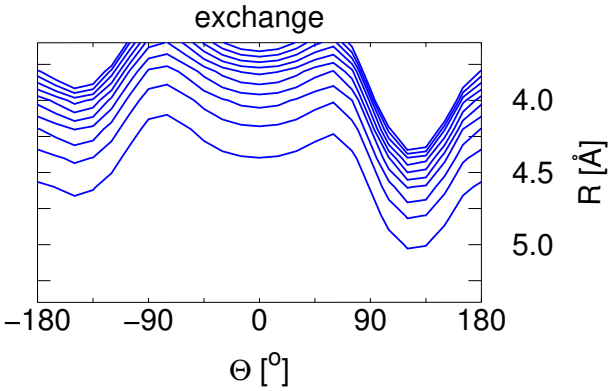

(b)

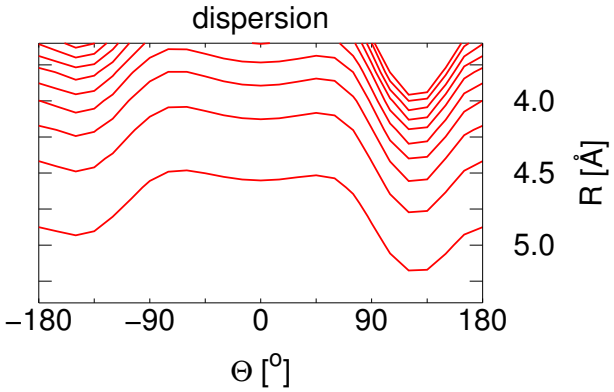

(c)

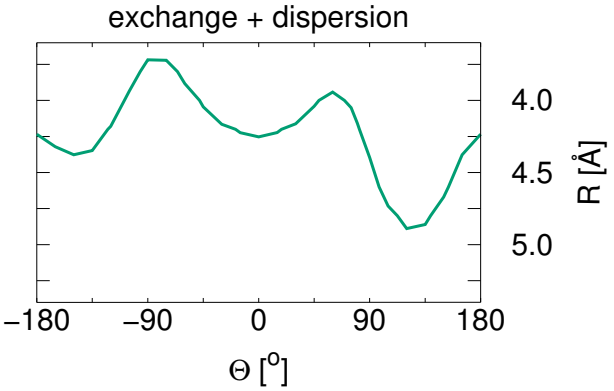

Figure 6
Georg Jansen, Stephan Schulz
J. Comput. Chem.

(a)

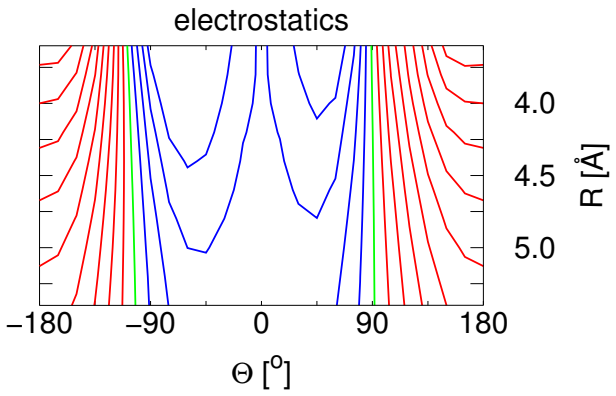

(b)

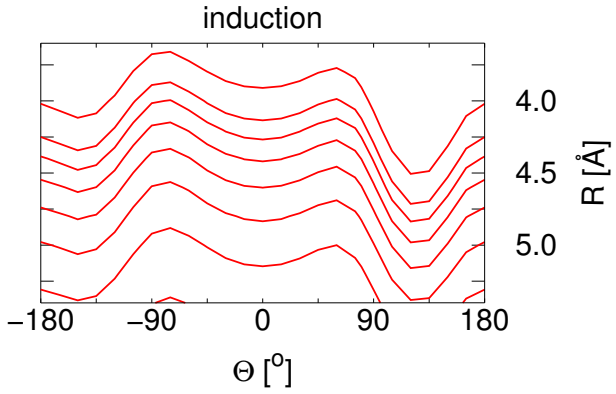

Figure 7
Georg Jansen, Stephan Schulz
J. Comput. Chem.

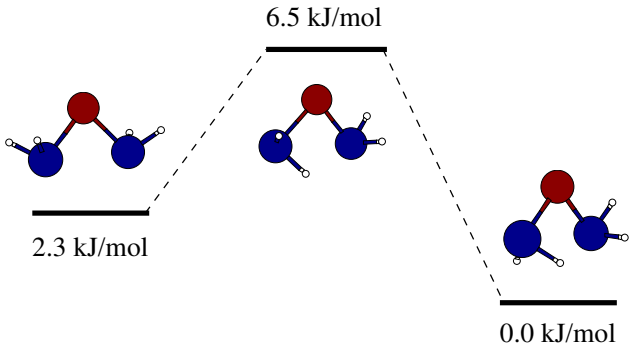

Figure 8
Georg Jansen, Stephan Schulz
J. Comput. Chem.

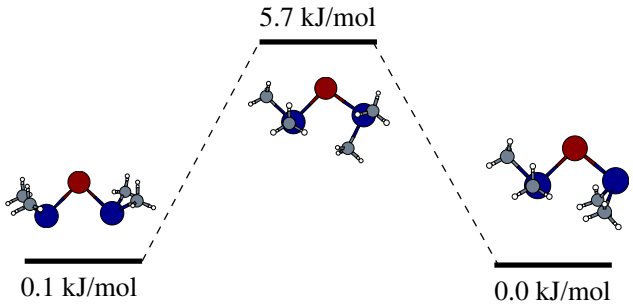

Figure 9
Georg Jansen, Stephan Schulz
J. Comput. Chem.

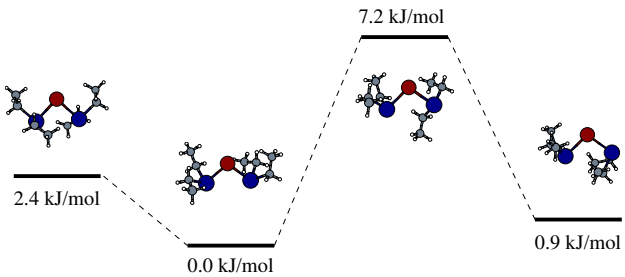

Figure 10
Georg Jansen, Stephan Schulz
J. Comput. Chem.

Method	**Basis set**	$\mathbf{R}_{\mathrm{Bi\cdots Bi}}$ [Å]			
		structure **A**	structure **B**	structure **C**	structure **D**
MP2	aVTZ	4.937	4.789	4.430	4.337
	aVQZ	4.937	4.773	4.424	4.332
	awCVTZ	4.528	4.521	4.209	4.178
	awCVQZ	4.484	4.485	4.176	4.152
SCS-MP2	aVTZ	5.121	4.940	4.552	4.450
	aVQZ	5.121	4.930	4.561	4.448
	aV5Z	5.121	4.927	4.563	4.446
	awCVTZ	4.740	4.697	4.361	4.307
	awCVQZ	4.707	4.670	4.335	4.296
	awCV5Z[a)]	4.713	4.696	4.337	4.294
CPC SCS-MP2	awCVTZ	4.802	4.754	4.412	4.354
	awCVQZ	4.741	4.702	4.365	4.302

Table 1: Bi$\cdots$Bi distances for the optimized structures of $(BiH_3)_2$. Eight electrons per monomer were correlated when using aVXZ basis sets, eighteen for awCVXZ. [a)] The highest angular momentum functions at Bi were left out in geometry optimizations for technical reasons.

Method	**Basis set**	$\mathbf{E}_{\mathrm{int}}$ [kJ/mol]			
		structure **A**	structure **B**	structure **C**	structure **D**
HF	awCV5Z	3.845	3.619	4.168	3.794
MP2	awCV5Z	-3.874	-6.792	-10.250	-11.517
	cbs(Q/5)	-3.980	-6.886	-10.393	-11.668
SCS-MP2	awCV5Z	-2.418	-4.811	-7.247	-8.325
	cbs(Q/5)	-2.430	-4.790	-7.371	-8.454
CCSD(T)	awCV5Z	-2.095	-4.780	-7.467	-8.430
	cbs(Q/5)	-2.174	-4.859	-7.593	-8.571

Table 2: Counterpoise-corrected interaction energies for the SCS-MP2/awCVTZ optimized structures of $(BiH_3)_2$.

Contribution	**E [kJ/mol]**			
	structure **A**	structure **B**	structure **C**	structure **D**
$E_{\mathrm{el}}^{(1)}$	-1.327	-3.697	-5.231	-8.706
$E_{\mathrm{exch}}^{(1)}$	3.227	7.346	10.313	14.981
$E_{\mathrm{ind}}^{(2)}$	-5.178	-6.531	-10.286	-19.466
$E_{\mathrm{ind-exch}}^{(2)}$	3.746	4.658	7.281	13.721
$E_{\mathrm{disp}}^{(2)}$	-5.482	-9.595	-13.584	-16.278
	(-5.744)	(-10.036)	(-14.205)	(-17.057)
$E_{\mathrm{disp-exch}}^{(2)}$	0.676	1.183	1.662	2.270
	(0.732)	(1.274)	(1.784)	(2.436)
$\delta(\mathrm{HF})$	2.829	1.729	2.221	4.732
E_{int}	-1.510	-4.907	-7.623	-8.747
	(-1.715)	(-5.257)	(-8.123)	(-9.359)

Table 3: DFT-SAPT/AQZVPP interaction energy contributions for the SCS-MP2/awCVTZ optimized structures of $(BiH_3)_2$. Values in parenthesis from ATZVPP/AQZVPP basis set extrapolation.

DOI: 10.1002/jcc.25209
URN: urn:nbn:de:hbz:464-20201215-144203-4

This is the peer reviewed version of the following article: Journal of Computational Chemistry 2018, Volume 39, Issue 20, Pages 1413 - 1423, which has been published in final form at: https://doi.org/10.1002/jcc.25209